

Spin-liquid phase in spin-1/2 square J_1 - J_2 Heisenberg model: A tensor product state approach

Ling Wang,¹ Zheng-Cheng Gu,² Frank Verstraete,¹ and Xiao-Gang Wen³

¹*Vienna Center for Quantum Science and Technology, Faculty of Physics,
University of Vienna, Boltzmannngasse 5, 1090 Vienna, Austria*

²*Kavli Institute for Theoretical Physics, University of California, Santa Barbara, CA 93106, USA*

³*Department of Physics, Massachusetts Institute of Technology, Cambridge, Massachusetts 02139, USA*
(Dated: March 13, 2012)

The ground state phase of spin-1/2 J_1 - J_2 antiferromagnetic Heisenberg model on square lattice in the maximally frustrated regime ($J_2 \sim 0.5J_1$) has been debated for decades. Here we study this model by using a recently proposed novel numerical method - the cluster update algorithm for tensor product states (TPSS). The ground state energies at finite sizes and in the thermodynamic limit (with finite size scaling) are in good agreement with the state of art exact diagonalization study, and the energy differences between these two studies are of the order of $10^{-3}J_1$ per site. At the largest bond dimension available D ($D = 9$), we find a paramagnetic ground state without any valence bond solid order in the thermodynamic limit in the range of $0.5 \leq J_2/J_1 \leq 0.6$, which implies the emergence of a spin-liquid phase. Furthermore, we investigate the topologically ordered nature of such a spin-liquid phase by measuring a nonzero topological entanglement entropy.

PACS numbers:

Introduction

The spin 1/2 J_1 - J_2 antiferromagnetic Heisenberg model on a square lattice has drawn great attention for the last two decades owing to its close relation to the disappearance of the antiferromagnetic (AF) long range order (LRO) in the high- T_c superconducting materials [1, 2], and has been proposed as a possible simple model to realize topologically ordered chiral spin-liquid state [3, 4] or Z_2 spin-liquid state [5–8]. The Hamiltonian of this model is given by:

$$H = J_1 \sum_{\langle i,j \rangle} \mathbf{S}_i \cdot \mathbf{S}_j + J_2 \sum_{\langle\langle i,j \rangle\rangle} \mathbf{S}_i \cdot \mathbf{S}_j, \quad (J_1, J_2 > 0), \quad (1)$$

where $\langle i, j \rangle$ represents the nearest neighbor (NN) pair and $\langle\langle i, j \rangle\rangle$ represents the next nearest neighbor (NNN) pair. For convenience, we set $J_1 = 1$ throughout the paper. It has long been believed that the frustration from NNN interaction competes with the NN one and drives the system through a quantum phase transition from an AF LRO phase to a magnetically disordered phase. In two extreme cases, the ground state phases of the model are well established: at very small J_2 , the ground state has AF LRO; and at very large J_2 , the system falls into two weakly coupled sets with magnetic susceptibility peaks at momentum $(\pi, 0)$ or $(0, \pi)$. In the intermediate coupling regime, quantum fluctuation is meant to destroy the AF LRO before the maximally frustrated point $J_2 = 0.5$ of the classical model and establishes a new paramagnetic phase. The nature of such a quantum phase is of great interest.

Numerous efforts have been made using many different approaches, such as the exact diagonalization (ED) [9–14], spin-wave theory [15, 16], series expan-

sion [17, 18], large- N expansion [19], the coupled cluster method (CCM) [20], variational methods (including short range resonating valence bond (SRVB) method) [21–23], and the fixed-node quantum monte carlo (QMC) [24]. Especially, a series expansion calculation of a general magnetic susceptibility over different perturbation fields suggests that within the Ginzburg-Landau paradigm the type of phase transition from the Néel to paramagnetic phase is of first order [18]. However, the same general magnetic susceptibility calculated with a coupled cluster method suggests a second order phase transition [20]. The debates about the phase near $J_2 = 0.5$ are more or less the same. A fixed-node QMC study indicates a plaquette valence bond solid (PVBS) state [24]; whereas the series expansion argues for a columnar valence bond solid (CVBS) state [18]. A relatively direct investigation of the nature of the ground state order is using the SRVB approximation [22], where with another term J_3 included in the Hamiltonian, a PVBS state along the line of $J_2 + J_3 = 0.5$ is found. It is worth to mention that the recent TPS studies have resolved a CVBS state [25], but with rather small bond dimension.

In this paper, we revisit this problem with a TPS [26] ansatz for the ground state wave function, accessed by the recently proposed cluster update algorithm [27], and reveal the answer to both questions. Up to $D = 9$, we observe a continuous phase transition from the Néel to paramagnetic phase at $J_2 = 0.5$. We further investigate the nature of the paramagnetic phase by measuring various VBS order parameters. Through finite size scaling (FSS), all considered VBS orders (including CVBS, staggered VBS (SVBS) and PVBS) scale to zero, implying the possible emergence of spin-liquid state. The exponentially decaying spin-spin and dimer-dimer correlation

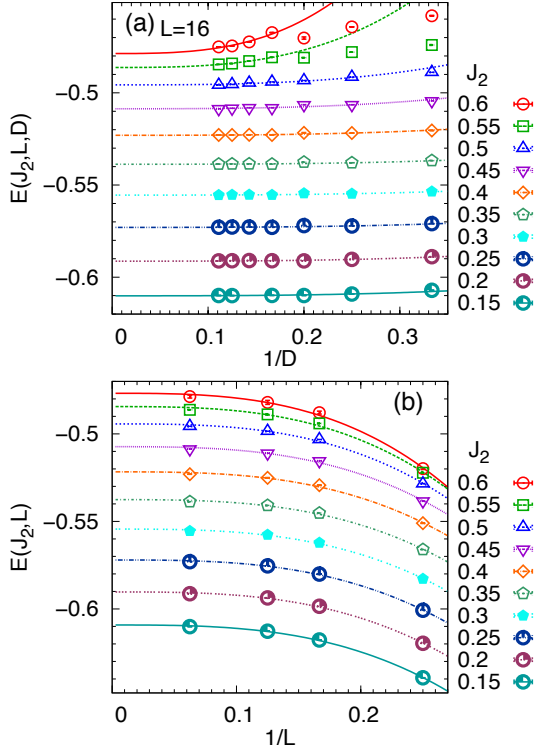


FIG. 1: (a) The finite size ($L = 16$) ground state energies at different bond dimensions $D = 3, 4, 5, 6, 7, 8, 9$, and their extrapolation (from ground energies at bond dimensions $D = 6, 7, 8, 9$) to $D \rightarrow \infty$ limit. (b) The finite size scaling of $E(J_2, L)$ obtained from (a) to the thermodynamic limit.

functions found in the paramagnetic phase indicate the non-zero spin and magnon excitation gaps. Moreover, we further verify the topologically ordered nature of such a spin-liquid phase by computing its constant part of Renyi entanglement entropy. Comparing to the previous studies in other systems [28, 29], our results provide stronger evidence for the existence of spin-liquid states in the spin $1/2$ J_1 - J_2 antiferromagnetic Heisenberg model on square lattice.

Results

We divide the square lattice into four sublattices A, B, C, D and associate each sublattice with a different tensor. Such a choice of tensor product state ansatz aims at describing all possible VBS orders and studying their competing effects. We use the cluster update imaginary time evolution method to evolve from a random TPS to the ground state of the above Hamiltonian. Upon obtaining the ground state TPS with bond dimension D up to 9, we evaluate the ground state energy, magnetization, dimer order and plaquette order parameters of a finite lattice with periodic boundary condition (PBC) of

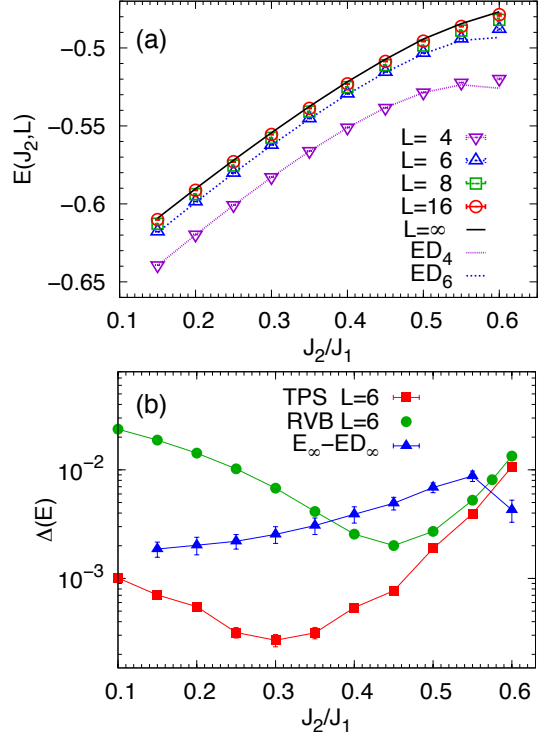


FIG. 2: (a) Finite size energies $E(J_2, L)$ obtained as in Fig. 1(a) and their thermodynamic limits $E(J_2)$ from the FSS in Fig. 1(b). The purple and blue dashed lines are the ED energies for lattice sizes $L = 4, 6$ respectively. (b) Energy absolute error per site for system size $L = 6$ as a function of J_2/J_1 compared between the TPSs study at bond dimension $D = 9$ (red squares) and a VMC study (green dots) with a RVB wavefunction ansatz [23]. The blue triangles are energy differences between $E(J_2)$ from the TPSs study and those extrapolated from an ED study up to 40 spins [14].

size $L \times L$ for $L = 4, 6, 8, 12, 16, 32$ based on the renormalization concept [30–32], using the monte carlo sampling technique [32]. We note that the TPS obtained from cluster imaginary time evolution method is indeed a variational state of an *infinite* system, however, it is very difficult [33] to evaluate the physical quantities for large systems with PBC. Here we evaluate them on relatively small size systems with high precision and then extrapolate to the thermodynamic limit.

We present the ground state energy for a finite lattice obtained from the TPSs of various bond dimensions D in Fig. 1(a). A clear decreasing of the ground state energy is observed when increasing bond dimension D , especially at $J_2 \in (0.45, 0.6)$. We thus extrapolate the finite size energy to the $D \rightarrow \infty$ limit with a formula

$$E(J_2, L, D) = E(J_2, L) + c_{J_2}/D^3, \quad (2)$$

here $E(J_2, L)$ and c_{J_2} are the fitting parameters. A finite size scaling formula [14, 34] is then employed to extrapo-

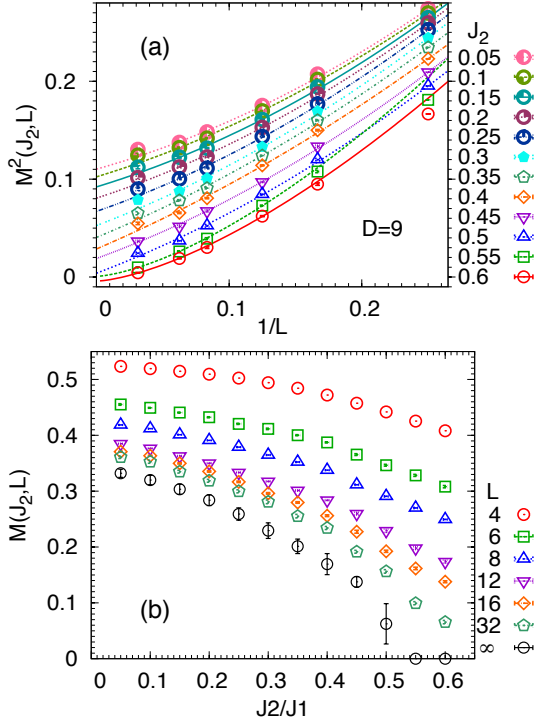


FIG. 3: (a) The FSS of the magnetization square to their thermodynamic limits. The maximal system size is 32×32 in this fitting. (b) The finite size magnetization $M(J_2, L)$ and their thermodynamic limits $M(J_2)$ obtained from (a) as a function of J_2/J_1 .

late the ground state energy in the thermodynamic limit,

$$E(J_2, L) = E(J_2) + d_{J_2}/L^3, \quad (3)$$

here $E(J_2)$ and d_{J_2} are the fitting parameters. The FSS results are presented in Fig. 1(b). The extrapolated finite size ground state energies together with their thermodynamic limits are plotted in Fig. 2(a). The difference between $E(J_2)$ and the thermodynamics limits obtained from a recent ED study [14] is plotted in Fig. 2(b). A good agreement (within the order of $5 \times 10^{-3} J_1$ per site) is reached between these two methods, whereas the rather large differences at $J_2 = 0.5, 0.55$ are caused by the unreliability of the ED extrapolation at these coupling strengths [14]. Fig. 2(b) also compares the absolute energy error per site for system size 6×6 obtained from the TPSs study at bond dimension $D = 9$ with the RVB variational MC results [23], a better achievement is obtained through the TPSs approach.

In the MC sampling scheme, the staggered magnetization square is evaluated as

$$M^2 = \frac{1}{N^2} \sum_{i,j=1}^N (-1)^{\phi_{ij}} \langle \mathbf{S}_{(x_i, y_i)} \cdot \mathbf{S}_{(x_j, y_j)} \rangle, \quad (4)$$

where $\phi_{ij} = x_i - x_j + y_i - y_j$ and (x_i, y_i) are the lattice coordinates of site i . We present the magnetization

results for finite size lattices in Fig. 3. Here the data presented are the results with the largest bond dimension available ($D = 9$) and without extrapolation over D , because the magnetization is not a monotonic function of D . A FSS formula [14, 34] is again employed to extrapolate the magnetization square in the thermodynamics limit,

$$M^2(J_2, L) = M^2(J_2) + e_{J_2}^1/L + e_{J_2}^2/L^2, \quad (5)$$

here $M^2(J_2)$, $e_{J_2}^1$ and $e_{J_2}^2$ are the fitting parameters. The FSS of the magnetization square is plotted in Fig. 3(a) and the magnetization at finite sizes and their thermodynamic limits are presented in Fig. 3(b). We observe that the magnetization decreases to zero at $J_2^c \approx 0.5$. This is clearly a sign of a continuous phase transition between the AF phase and the paramagnetic phase. To encounter a different asymptotic behavior in the paramagnetic phase, we employ a slightly different fitting formula for the finite size magnetization square $M^2(J_2, L) = M^2(J_1) + e_{J_2}^3/L^{1.5}$. The power law (exponentially) decaying spin-spin correlation function at $J_2 = 0.5$ ($J_2 = 0.55$) is another proof for the disappearing of the staggered magnetization on and after the critical point $J_2^{c1} \approx 0.5$ (see supplemental material Fig. 8).

To further determine the phase at the paramagnetic region $J_2 \in [0.5, 0.6]$, several order parameters are investigated. We define the CVBS orders as

$$M_{dx}^2 = \frac{1}{N^2} \sum_{i,j=1}^N (-1)^{x_i - x_j} \langle D_i^x D_j^x \rangle, \quad (6)$$

$$M_{dy}^2 = \frac{1}{N^2} \sum_{i,j=1}^N (-1)^{y_i - y_j} \langle D_i^y D_j^y \rangle; \quad (7)$$

and the SVBS orders as

$$M_{sx}^2 = \frac{1}{N^2} \sum_{i,j=1}^N (-1)^{\phi_{ij}} \langle D_i^x D_j^x \rangle, \quad (8)$$

$$M_{sy}^2 = \frac{1}{N^2} \sum_{i,j=1}^N (-1)^{\phi_{ij}} \langle D_i^y D_j^y \rangle, \quad (9)$$

here $D_i^\alpha = \mathbf{S}_{(x_i, y_i)} \cdot \mathbf{S}_{(x_i, y_i) + \vec{\alpha}}$, ($\vec{\alpha} = \vec{x}, \vec{y}$) and $\phi_{ij} = x_i - x_j + y_i - y_j$. We also define the PVBS orders as [22]

$$M_Q^2 = \frac{1}{N^2} \sum_{i,j=1}^N (-1)^{\phi_{ij}} (\langle Q_i Q_j \rangle - \langle Q_i \rangle \langle Q_j \rangle), \quad (10)$$

here $Q_i \equiv \frac{1}{2}(P_{\square_i} + P_{\square_i}^{-1})$ is the permutation operator that permutes the 4 spins on a plaquette.

Fig. 4 and Fig. 5 demonstrate the CVBS, SVBS and PVBS orders respectively as a function of inverse lattice size L evaluated using TPSs at bond dimension $D = 9$. Through FSS, we find all of them scale to zero in the thermodynamic limit. This result rules out the VBS as a

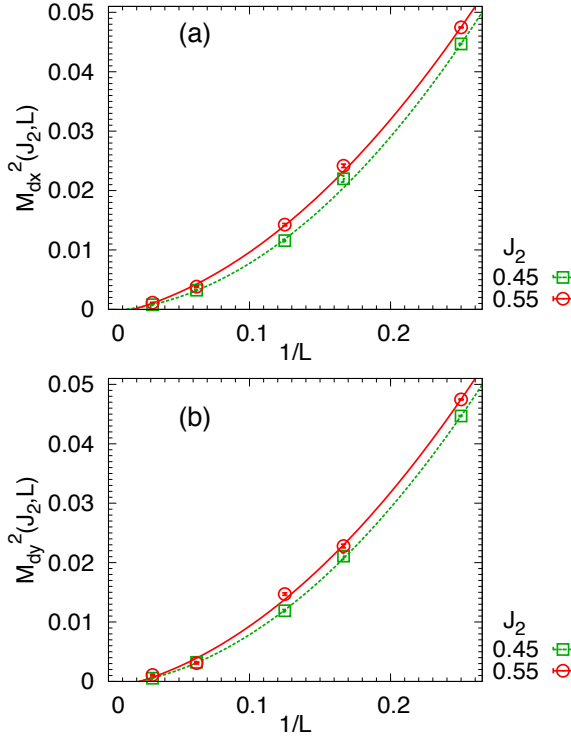


FIG. 4: The CVBS order parameter (a) M_{dx}^2 and (b) M_{dy}^2 as a function of inverse system length $1/L$ fitted using a second-order polynomials, evaluated from TPSs of bond dimension $D = 9$ at $L = 4, 6, 8, 16, 32$.

candidate for the ground state of the paramagnetic phase, and the most possible state of the paramagnetic phase is a spin-liquid state. We further compute the real space spin-spin and dimer-dimer correlation functions (see supplementary material) and find all of them decay exponentially with distance in the paramagnetic phase, implying the gaped spin-liquid nature of the observed paramagnetic phase. Moreover, a metastable state (see Fig. 1, which has slightly higher variational energy) with coexisting CVBS and SVBS orders is observed at $D \leq 4$ (see supplementary material), which is consistent with previous study [25] and implies the emergence of the spin-liquid phase as a consequence of melting various VBS orders.

To determine whether the observed paramagnetic phase is topologically ordered or not and what kind of topological order it is, we further compute the Renyi entanglement entropy $S_2(L)$ between two $L \times L$ subsystems by cutting a $2L \times L$ torus into equal size halves. The entanglement entropy for a cylindrical geometry is presented in Fig. 6(a). Through extrapolation we could isolate the the constant term of the Renyi entanglement entropy S_2 of the paramagnetic phase. It has been shown that the translational invariant TPS (with a 2 by 2 unit cell) ansatz belongs to a special topological sector of the degenerate ground states and the Renyi entanglement entropy S_2 will scale as $S_2 = \alpha L - \gamma$ [35–39], where γ is

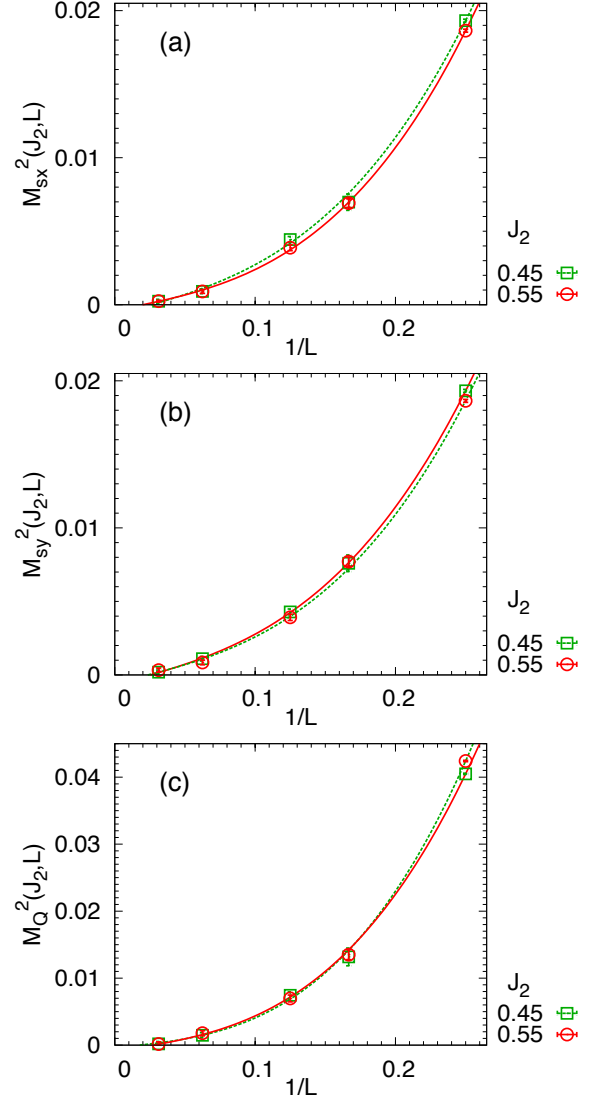


FIG. 5: The SVBS order parameter (a) M_{sx}^2 , (b) M_{sy}^2 and (c) the PVBS order parameter M_Q^2 as a function of inverse system length $1/L$ fitted using a third-order polynomials, evaluated from TPSs of bond dimension $D = 9$ at $L = 4, 6, 8, 16, 32$.

a universal constant - the topological entanglement entropy. We find that in the paramagnetic phase γ reaches a conspicuously large value between 0.8 and 1.3. One possible candidate for the paramagnetic phase, the gaped Z_2 spin-liquid [6, 40], has a topological entanglement entropy equal to $\ln 2 \sim 0.69$ [35, 36], which happens to be close to the calculated intersection. As an additional check, we also calculate the Renyi entanglement entropy between a square of size $L \times L$ and the rest of the system on a 16×16 lattice for $L \in [3 : 8]$. The Renyi entanglement entropy for such a disk geometry is presented in Fig. 6(b). We also find a nonzero intersection in this case, however, due to the non-universal corner entropy contributions, the actual value has a small difference.

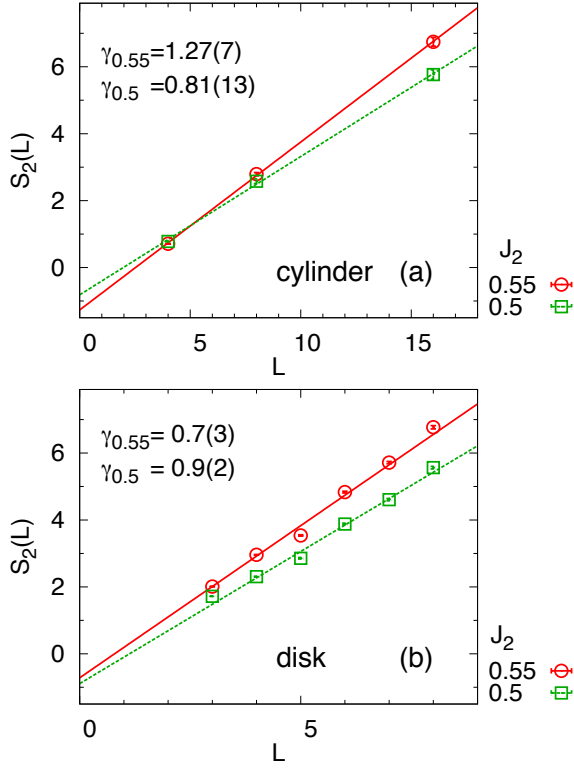


FIG. 6: (a) The Renyi entropy $S_2(L)$ between two $L \times L$ subsystems by cutting a $2L \times L$ torus into halves, evaluated from TPSs of bond dimension $D = 9$ at $L = 4, 8, 16$. (b) The Renyi entropy $S_2(L)$ between a $L \times L$ disk subsystem and the rest of a 16×16 torus, evaluated from TPSs of bond dimension $D = 9$ for $L \in [3 : 8]$.

Conclusions and discussions

In conclusion, we applied the cluster update algorithm for TPSs to study the frustrated spin $1/2$ J_1 - J_2 antiferromagnetic Heisenberg model on square lattice. Limited to a cluster size 2×2 , a rather large bond dimension $D = 9$ is feasible. Through a finite D scaling and finite size scaling (FSS), our ground state energies at finite sizes and in the thermodynamic limit are in good agreement with the results from a state of art ED study [14], with a difference at an order of $10^{-3}J_1$ per site. Through FSS, the staggered magnetization diminishes to zero at $J_2^{c1} \approx 0.5$, suggesting a continuous quantum phase transition at a critical point $J_2^{c1} \approx 0.5$. We further determined the nature of the paramagnetic phase using 3 sets of order parameters: the columnar dimer order M_{dx}^2 and M_{dy}^2 , the staggered dimer order M_{sx}^2 and M_{sy}^2 , and the plaquette order M_Q^2 . At a large bond dimension D ($D = 9$), we found that all these order parameters scale to zero in the thermodynamic limit, which ruled out the columnar, staggered and plaquette dimer orders. We computed the constant part of the Renyi entanglement entropy for

the paramagnetic phase, and found strong evidence to support the possibility of being a spin-liquid. In principle, the complete topological information characterized by the fractional statistics of quasiparticles can be read out through a renormalization scheme[41] for the TPS ansatz. A detailed study along this direction will be presented in our future work.

Method

The cluster update imaginary time evolution algorithm

The following is an illustration of how to construct the evolution operators for this Hamiltonian. We expand the evolution operator $\hat{O} \sim \exp\{-\epsilon J_1(\mathbf{S}_1 \cdot \mathbf{S}_2 + \mathbf{S}_2 \cdot \mathbf{S}_3) - 2\epsilon J_2 \mathbf{S}_1 \cdot \mathbf{S}_3\}$ on 3 sites from the Trotter decomposition of the partition function. By writing $\exp(-\epsilon J \mathbf{S}_i \cdot \mathbf{S}_j)$ as

$$\prod_{\alpha} [\cosh(\epsilon J/4) \mathbb{1}_i \otimes \mathbb{1}_j - \sinh(\epsilon J/4) \sigma_i^{\alpha} \otimes \sigma_j^{\alpha}], \quad (11)$$

where $\alpha = x, y, z$, σ^{α} are Pauli matrices, and omitting higher orders of $O(\epsilon)$, one obtains

$$\begin{aligned} \hat{O} = & \mathbb{1}_1 \otimes \mathbb{1}_2 \otimes \mathbb{1}_3 - \sum_{\alpha} \tanh(\epsilon J_1/4) \sigma_1^{\alpha} \otimes \sigma_2^{\alpha} \otimes \mathbb{1}_3 \\ & - \sum_{\alpha} \tanh(\epsilon J_1/4) \mathbb{1}_1 \otimes \sigma_2^{\alpha} \otimes \sigma_3^{\alpha} \\ & - \sum_{\alpha} \tanh(\epsilon J_2/2) \sigma_1^{\alpha} \otimes \mathbb{1}_2 \otimes \sigma_3^{\alpha}. \end{aligned} \quad (12)$$

The above terms can be expressed as a matrix product operator (MPO) [42],

$$\begin{aligned} \hat{O} = & \sum_{i_1, i_2, i_3=0}^3 (\mathbf{v}_{i_1}^T \mathbf{B}_{i_2} \mathbf{v}_{i_3}) \mathbf{X}_{i_1} \otimes \mathbf{X}_{i_2} \otimes \mathbf{X}_{i_3} \\ \mathbf{X}_0 = & \mathbb{1}, \quad \mathbf{X}_1 = \sigma^x, \quad \mathbf{X}_2 = \sigma^y, \quad \mathbf{X}_3 = \sigma^z, \\ \mathbf{v}_0 = & |0\rangle, \\ \mathbf{v}_i = & a|i\rangle, \quad (i = 1, 2, 3), \\ \mathbf{B}_0 = & |0\rangle\langle 0| + b|1\rangle\langle 1| + b|2\rangle\langle 2| + b|3\rangle\langle 3|, \\ \mathbf{B}_i = & c|0\rangle\langle i| + c|i\rangle\langle 0|, \quad (i = 1, 2, 3), \end{aligned} \quad (13)$$

where \mathbf{v}_i are the vectors of length 4, \mathbf{B}_i are 4×4 matrices, \mathbf{X}_i are operators acting on the physical index, and a, b, c are scalar variables. In order to correctly match the coefficients in front of each term in Eq. (12), a, b, c have to be chosen to satisfy $ac = -\tanh(\epsilon J_1/4)$, $a^2b = -\tanh(\epsilon J_2/2)$, and $|a|, |b|, |c| \ll 1$. Thus the evolution operators on these sites are written as $\hat{O}_1 = \sum_i \mathbf{v}_i^T \otimes \mathbf{X}_i$, $\hat{O}_2 = \sum_i \mathbf{B}_i \otimes \mathbf{X}_i$ and $\hat{O}_3 = \sum_i \mathbf{v}_i \otimes \mathbf{X}_i$ respectively.

We present the diagrammatic representation of the evolution operators \hat{O}_1 , \hat{O}_2 and \hat{O}_3 acting on sites A , B and C in a 2×2 cluster in Fig. 7(b). The corresponding simple update scheme is sketched in Fig. 7(a). In

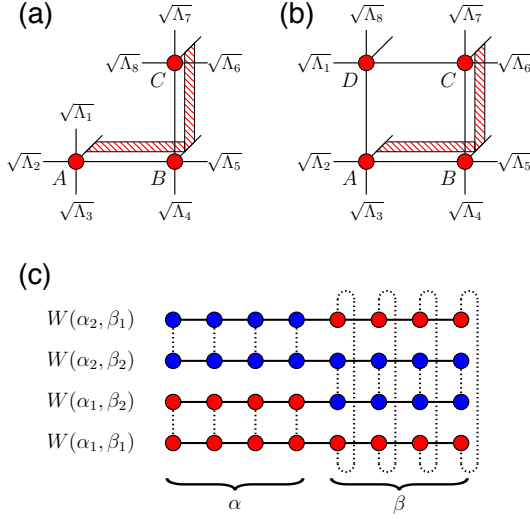


FIG. 7: (a) The simple update scheme. (b) The cluster update scheme with a cluster size 2×2 . (c) A illustration of the MC sampling of the swap operator to measure the Renyi entanglement entropy S_2 of a subset β for a 1 dimension system using 2 copies (represented by red and blue dots respectively) of the system. Dashed lines indicate summing over the spin degrees of freedom. $W(\alpha_i, \beta_i)$ is the weight of the spin configuration (α_i, β_i) calculated using a tensor RG contraction scheme in 2 dimension.

both cases, the complexity scales as D^5 , and there is no cumulative error.

Monte Carlo sampling of Renyi entanglement entropy

The Renyi entanglement entropy $S_2(L)$ can be measured via Monte Carlo sampling of the swap operator using two copies of the system [43], as demonstrated in Fig. 7(c),

$$\langle Swap \rangle = \frac{\sum_{\sigma_1, \sigma_2} W^2(\sigma_1) W^2(\sigma_2) Swap(\sigma_1, \sigma_2)}{\sum_{\sigma_1, \sigma_2} W^2(\sigma_1) W^2(\sigma_2)},$$

$$Swap(\sigma_1, \sigma_2) = \frac{W(\alpha_1, \beta_2) W(\alpha_2, \beta_1)}{W(\alpha_1, \beta_1) W(\alpha_2, \beta_2)}, \quad (14)$$

where $\sigma_i \equiv (\alpha_i, \beta_i)$, α_i, β_i are the spin configurations of the left and right halves of the copy i , and $W(\alpha_i, \beta_j)$ is the coefficient of the spin configuration (α_i, β_j) , which can be evaluated using a tensor RG contraction scheme [31, 32].

Acknowledgments

We would like to thank J. Richter for passing their exact diagonalization data for comparison, thank F. Becca

for passing their variational monte carlo data for comparison; and thank A. W. Sandvik, Leon Balents and H.-C. Jiang for their stimulating discussion. This project is supported by the EU Strep project QUEVADIS, the ERC grant QUERG, and the FWF SFB grants FoQuS and ViCoM. Z.C.G. is partly supported by NSF Grant No. PHY05-51164. The computational results presented have been achieved using the Vienna Scientific Cluster (VSC).

Note added.— After the completion of our work, we learned that Hong-Chen Jiang, Hong Yao and Leon Balents obtained similar results [44] from high precision DMRG calculation.

-
- [1] P. W. Anderson The resonating valence bond state in La_2CuO_4 and superconductivity, *Science* **235**, 1196 (1987).
 - [2] For a review, see P. A. Lee, N. Nagaosa and X. G. Wen, Doping a Mott insulator: Physics of high-temperature superconductivity, *Phys. Mod. Phys.* **78**, 17 (2006).
 - [3] V. Kalmeyer and R. B. Laughlin, Equivalence of the resonating-valence-bond and fractional quantum Hall states, *Phys. Rev. Lett.* **59**, 2095 (1987).
 - [4] X.-G. Wen, F. Wilczek and A. Zee, Chiral Spin States and Superconductivity, *Phys. Rev. B* **39**, 11413(1989).
 - [5] N. Read and S. Sachdev, Large-N expansion for frustrated quantum antiferromagnets, *Phys. Rev. Lett.* **66**, 1773 (1991).
 - [6] X.-G. Wen, Mean Field Theory of Spin Liquid States with Finite Energy Gaps and Topological Order, *Phys. Rev. B* **44**, 2664 (1991).
 - [7] R. Moessner and S. L. Sondhi, Resonating Valence Bond Phase in the Triangular Lattice Quantum Dimer Model, *Phys. Rev. Lett.* **86**, 1881 (2001).
 - [8] Hong Yao, and S. A. Kivelson, Exact Spin Liquid Ground States of the Quantum Dimer Model on the Square and Honeycomb Lattices, (2011), arXiv:1112.1702(unpublished).
 - [9] E. Dagotto and A. Moreo, Phase diagram of the frustrated spin-1/2 Heisenberg antiferromagnet in 2 dimensions, *Phys. Rev. Lett.* **63**, 2148 (1989).
 - [10] F. Figueirido, A. Karlhede, S. Kivelson, S. Sondhi, M. Rocek and D. S. Rokhsar, Exact diagonalization of finite frustrated spin-1/2 Heisenberg models, *Phys. Rev. B* **41**, 4619 (1990).
 - [11] H. J. Schulz and T. A. L. Ziman, Finite-Size Scaling for the Two-Dimensional Frustrated Quantum Heisenberg Antiferromagnet, *Europhys. Lett.* **18**, 355 (1992).
 - [12] H. J. Schulz, T. A. L. Ziman and D. Poilblanc, Magnetic Order and Disorder in the Frustrated Quantum Heisenberg Antiferromagnet in Two Dimensions, *J. Phys. I* **6**, 675 (1996).
 - [13] T. Einarsson and H. J. Schulz, Direct calculation of the spin stiffness in the J_1 - J_2 Heisenberg antiferromagnet, *Phys. Rev. B* **51**, 6151 (1995).
 - [14] J. Richter and J. Schulenburg, The spin-1/2 J_1 - J_2 Heisenberg antiferromagnet on the square lattice: Exact diagonalization for N=40 spins, *Eur. Phys. J. B* **73**, 117 (2010).

- [15] P. Chandra and B. Douçot, Possible spin-liquid state at large S for the frustrated square Heisenberg lattice, *Phys. Rev. B* **38**, 9335 (1988).
- [16] N. B. Ivanov and P. Ch. Ivanov, Frustrated two-dimensional quantum Heisenberg antiferromagnet at low temperatures, *Phys. Rev. B* **46**, 8206 (1992).
- [17] M. Arlego and W. Brenig, Plaquette order in the J_1 - J_2 - J_3 model: Series expansion analysis, *Phys. Rev. B* **78**, 224415 (2008).
- [18] J. Sirker, Z. Weihong, O. P. Sushkov and J. Oitmaa, J_1 - J_2 model: First-order phase transition versus deconfinement of spinons, *Phys. Rev. B* **73**, 184420 (2006).
- [19] N. Read and S. Sachdev, Large- N expansion for frustrated quantum antiferromagnets, *Phys. Rev. Lett.* **66**, 1773 (1991).
- [20] R. Darradi, O. Derzhko, R. Zinke, J. Schulenburg, S. E. Krüger and J. Richter, Ground state phases of the spin-1/2 J_1 - J_2 Heisenberg antiferromagnet on the square lattice: A high-order coupled cluster treatment, *Phys. Rev. B* **78**, 214415 (2008).
- [21] K. S. D. Beach, Master equation approach to computing RVB bond amplitudes, *Phys. Rev. B* **79**, 224431 (2009).
- [22] M. Mambrini, A. Läuchli, D. Poilblanc and F. Mila, Plaquette valence-bond crystal in the frustrated Heisenberg quantum antiferromagnet on the square lattice, *Phys. Rev. B* **74**, 144422 (2006).
- [23] L. Capriotti, F. Becca, A. Parola and S. Sorella, Resonating Valence Bond Wave Functions for Strongly Frustrated Spin Systems, *Phys. Rev. Lett.* **87**, 097201 (2001).
- [24] L. Capriotti and S. Sorella, Spontaneous Plaquette Dimerization in the J_1 - J_2 Heisenberg Model, *Phys. Rev. Lett.* **84**, 3173 (2000).
- [25] V. Murg, F. Verstraete and J. I. Cirac, Exploring frustrated spin systems using projected entangled pair states, *Phys. Rev. B* **79**, 195119 (2009).
- [26] F. Verstraete, and J. I. Cirac, Renormalization algorithms for Quantum-Many Body Systems in two and higher dimensions, (2004), arXiv:cond-mat/0407066v1.
- [27] L. Wang, and F. Verstraete, Cluster update for tensor network states, (2011), arXiv:1110.4362(unpublished).
- [28] Z. Y. Meng, T. C. Lang, S. Wessel, F. F. Assaad and A. Muramatsu, Quantum spin liquid emerging in two-dimensional correlated Dirac fermions, *Nature* **464**, 847 (2010).
- [29] Simeng Yan, D. A. Huse, and S. R. White, Spin-Liquid Ground State of the $S = 1/2$ Kagome Heisenberg Antiferromagnet, *Science* **332**, 1173 (2011).
- [30] M. Levin and C. P. Nave, *Phys. Rev. Lett.* **99**, Tensor renormalization group approach to 2D classical lattice models, 120601 (2007).
- [31] Z.-C. Gu, M. Levin, and X.-G. Wen, Tensor-entanglement renormalization group approach as a unified method for symmetry breaking and topological phase transitions, *Phys. Rev. B* **78**, 205116 (2008).
- [32] L. Wang, I. Pižorn and F. Verstraete, Monte Carlo simulation with tensor network states, *Phys. Rev. B* **83**, 134421 (2011).
- [33] F. Verstraete, M. M. Wolf, D. Perez-Garcia and J. I. Cirac, Criticality, the Area Law, and the Computational Power of Projected Entangled Pair States, *Phys. Rev. Lett.* **96**, 220601 (2006).
- [34] A. W. Sandvik, Finite-size scaling of the ground-state parameters of the two-dimensional Heisenberg model, *Phys. Rev. B* **56**, 11678 (1997).
- [35] A. Kitaev and J. Preskill, Topological entanglement entropy, *Phys. Rev. Lett.* **96**, 110404 (2006).
- [36] M. Levin and X.-G. Wen, Detecting topological order in a ground state wave function, *Phys. Rev. Lett.* **96**, 110405 (2006).
- [37] S. T. Flammia, Alioscia Hamma, Taylor L. Hughes and X.-G. Wen, Topological Entanglement Renyi Entropy and Reduced Density Matrix Structure, *Phys. Rev. Lett.* **103**, 261601 (2009).
- [38] Z. C. Gu, Michael Levin, Brian Swingle and X.-G. Wen, Tensor-product representations for string-net condensed states, *Phys. Rev. B* **79**, 085118 (2009).
- [39] Tarun Grover, Quantum Entanglement and Detection of Topological Order in Numerics, (2011), arXiv:1112.2215(unpublished).
- [40] X.-G. Wen, Quantum Orders and Symmetric Spin Liquids, *Phys. Rev. B* **65**, 165133 (2002).
- [41] Xie Chen, Z.-C. Gu, and X.-G. Wen, Local unitary transformation, long-range quantum entanglement, wave function renormalization, and topological order, *Phys. Rev. B* **82**, 155138 (2010).
- [42] B. Pirvu, V. Murg, J. I. Cirac and F. Verstraete, Matrix product operator representations, *New J. Phys.* **12**, 025012 (2010).
- [43] M. Hastings, I. Gonzalez, A. B. Kallin and R. Melko, Measuring Renyi Entanglement Entropy in Quantum Monte Carlo Simulations, *Phys. Rev. Lett.* **104**, 157201 (2010).
- [44] H. C. Jiang, Hong Yao, and Leon Balents, Spin Liquid Ground State of the Spin-1/2 Square J_1 - J_2 Heisenberg Model, (2011), arXiv:1112.2241(unpublished).

Supplementary material

The spin-spin and dimer-dimer correlation functions

We further calculate the spin-spin and dimer-dimer correlation functions at both critical point and deep in the paramagnetic region. Define

$$C(r, 0) = \langle \mathbf{S}_{(0,0)} \cdot \mathbf{S}_{(r,0)} \rangle, \quad (15)$$

$$C_{dx}(r, 0) = \langle D_0^x D_r^x \rangle, \quad (16)$$

we found the spin-spin correlation $(-1)^r C(r, 0)$ decays as a power law $r^{-\alpha_s}$ at the critical point with an exponent $\alpha_s = 1.31(3)$, however decays exponentially e^{-r/ξ_s} in the paramagnetic region with a spin correlation length $\xi_s =$

2.6(1); and the dimer-dimer correlation $(-1)^r C_{dx}(r, 0)$ decays as a power law $r^{-\alpha_d}$ at the critical point with an exponent $\alpha_d = 3.0(3)$, while decays exponentially e^{-r/ξ_d} in the paramagnetic region with a dimer correlation length $\xi_d = 1.49(1)$, as demonstrated in Fig. 8 and Fig. 9. This indicates that the paramagnetic phase has both spin $S = 0$ gap and spin $S = 1$ gap.

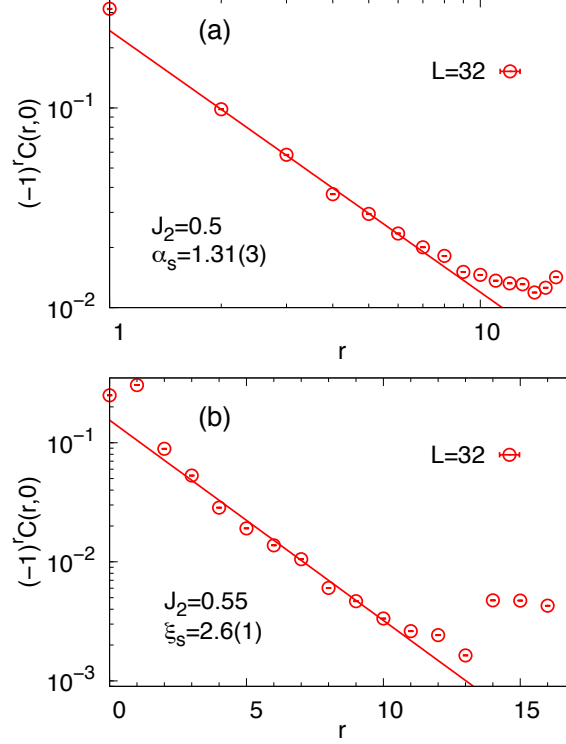


FIG. 8: The spin-spin correlation as a function of separation r at (a) $J_2 = 0.5$ and (b) $J_2 = 0.55$. At the critical point $J_2 = 0.5$, $(-1)^r C(r, 0)$ decays as power law $r^{-\alpha_s}$ with $\alpha_s = 1.31(3)$, while at $J_2 = 0.55$, $(-1)^r C(r, 0)$ decays exponentially as e^{-r/ξ_s} with a spin correlation length $\xi_s = 2.6(1)$.

Observation of VBS order at small bond dimension $D < 5$

In addition to the squared VBS orders, we also define the average of the dimer orders to detect if the symmetry is broken or not;

$$\begin{aligned} D_{dx} &= \sum_i (-1)^{x_i} \langle D_i^x \rangle, & D_{dy} &= \sum_i (-1)^{y_i} \langle D_i^y \rangle; \\ D_{sx} &= \sum_i (-1)^{x_i+y_i} \langle D_i^x \rangle, & D_{sy} &= \sum_i (-1)^{x_i+y_i} \langle D_i^y \rangle. \end{aligned} \quad (17)$$

Fig. 10 shows the absolute value of the average order parameters as a function of J_2/J_1 at bond dimension $D = 4$. We find that the paramagnetic ground state has nonzero D_{dx} , D_{dy} and D_{sy} of a magnitude 10^{-2} , which indicates a mixed columnar and staggered VBS orders. However, after $D \geq 5$, all of them disappear when ground state energy further decreases (see in Fig. 1 for a comparison of energies at different bond dimensions D), implying the local minimal effects of these ordered states. The observed VBS orders for small D are a consequence of spontaneous symmetry breaking. However if increasing the bond dimension D , all average order parameters become zero, which indicates a restoration of certain broken symmetries caused by the restriction of bond dimension D .

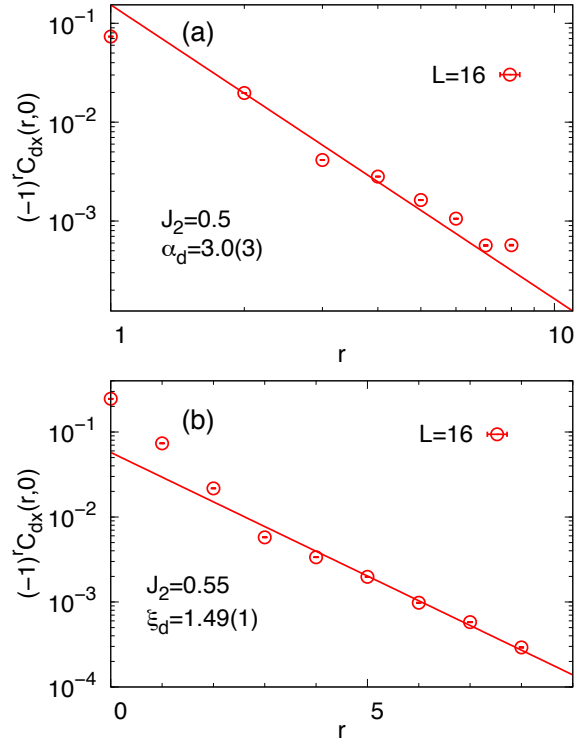


FIG. 9: The dimer-dimer correlation as a function of separation r at (a) $J_2 = 0.5$ and (b) $J_2 = 0.55$. At the critical point $J_2 = 0.5$, $(-1)^r C_{dx}(r, 0)$ decays as power law $r^{-\alpha_d}$ with $\alpha_d = 3.0(3)$, while at $J_2 = 0.55$, $(-1)^r C_{dx}(r, 0)$ decays exponentially as e^{-r/ξ_d} with a dimer correlation length $\xi_d = 1.49(1)$.

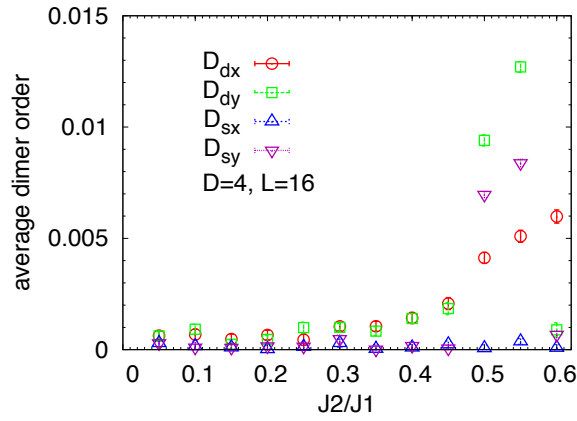


FIG. 10: The average columnar dimer order D_{dx} , D_{dy} and staggered dimer order D_{sx} , D_{sy} (defined in Eq. 17) as a function of J_2/J_1 at bond dimension $D = 4$ for system size $L = 16$.